Molecular Therapy
Nucleic Acids
Original Article

CRISPR-Cas9 editing of a TNPO3 mutation in a muscle cell model of limb-girdle muscular dystrophy type D2

Javier Poyatos-García,[1,2,9] Águeda Blázquez-Bernal,[3,4,9] Marta Selva-Giménez,[1,2] Ariadna Bargiela,[2] Jorge Espinosa-Espinosa,[3,4] Rafael P. Vázquez-Manrique,[1,5,6] Anne Bigot,[7] Ruben Artero,[3,4,8] and Juan Jesús Vilchez[1,2,8]

[1]Centre for Biomedical Network Research on Rare Diseases (CIBERER), U763, CB06/05/0091, 46026 Valencia, Spain; [2]Neuromuscular and Ataxias Research Group, Health Research Institute Hospital La Fe (IIS La Fe), 46026 Valencia, Spain; [3]Translational Genomics Group, University Institute for Biotechnology and Biomedicine (BIOTECMED), University of Valencia, Burjasot, 46100 Valencia, Spain; [4]INCLIVA Biomedical Research Institute, 46010 Valencia, Spain; [5]Grupo de Investigación en Biomedicina Molecular, Celular y Genómica, Instituto de Investigación Sanitaria La Fe (IIS La Fe), 46026 Valencia, Spain; [6]Joint Unit for Rare Diseases IIS La Fe-CIPF, 46012 Valencia, Spain; [7]Sorbonne Université, INSERM, Institut de Myologie, Centre de Recherche en Myologie, 75013 Paris, France

A single-nucleotide deletion in the stop codon of the nuclear import receptor transportin-3 (TNPO3), also involved in human immunodeficiency virus type 1 (HIV-1) infection, causes the ultrarare autosomal dominant disease limb-girdle muscular dystrophy D2 (LGMDD2) by extending the wild-type protein. Here, we generated a patient-derived *in vitro* model of LGMDD2 as an immortalized myoblast cell line carrying the *TNPO3* mutation. The cell model reproduced critical molecular alterations seen in patients, such as *TNPO3* overexpression, defects in terminal muscle markers, and autophagy overactivation. Correction of the *TNPO3* mutation via CRISPR-Cas9 editing caused a significant reversion of the pathological phenotypes in edited cells, including a complete absence of the mutant TNPO3 protein, as detected with a polyclonal antibody specific against the abnormal 15-aa peptide. Transcriptomic analyses found that 15% of the transcriptome was differentially expressed in model myotubes. CRISPR-Cas9-corrected cells showed that 44% of the alterations were rescued toward normal levels. MicroRNAs (miRNAs) analyses showed that around 50% of miRNAs with impaired expression because of the disease were recovered on the mutation edition. In summary, this work provides proof of concept of the potential of CRISPR-Cas9-mediated gene editing of *TNPO3* as a therapeutic approach and describes critical reagents in LGMDD2 research.

INTRODUCTION

Limb-girdle muscular dystrophy type D2 (LGMDD2; OMIM: 608423), is a rare genetic disease for which there is currently no effective treatment. LGMDD2 is characterized by progressive muscle weakness and atrophy of proximal and distal muscles, generalized contractures, and skeletal deformities.[1,2] Remarkable features of this autosomal dominant disorder are its broad range of onset (congenital to adulthood) and variable degree of severity and progression. One of the mutations leading to LGMDD2 was a single adenine nucleotide deletion (*c.2771delA*) in the C-terminal region of the transportin-3 (*TNPO3*) gene, causing a frameshift that abolishes the terminal stop codon generating a mutant transportin (TNPO3mut) with a 15-aa extension (CSHSCTVPVTQECLF),[2,3] which is co-expressed with the wild-type TNPO3 (TNPO3wt) protein. Additional *TNPO3* mutations (*c.2767delC* and *c.2757delC*) have been reported,[4,5] leading to elongated proteins. The known mutant TNPO3 proteins share the same 14-aa C-terminal extension, suggesting that this peptide, rather than the specific mutation, triggers the disease.[6] An additional *TNPO3* missense mutation (*c.2453G>A*) with a different impact on the structure was found in a sporadic case whose phenotype differs essentially from the typical LGMDD2.[7]

TNPO3 is a β-importin responsible for the nuclear import of serine/arginine-rich (SR) proteins essential for alternative RNA splicing and polyadenylation.[8,9] It is also required for human immunodeficiency virus type 1 (HIV-1) infection; indeed, the *TNPO3 c.2771delA* mutation interferes significantly with this process, protecting LGMDD2 cells patients against HIV-1 infection.[10] *Drosophila* human TNPO3mut expression with concomitant silencing of the endogenous fly protein ortholog reproduced critical aspects of the disease. Notably, a TNPO3 protein increase has been reported in the somatic musculature of model flies,[6] consistent with observations in LGMDD2 muscle samples.[4] TNPO3 is involved in myogenesis as TNPO3 levels, and subcellular localization changed during the myogenic process and myotube differentiation.[11] However, the

Received 28 March 2022; accepted 6 January 2023;
https://doi.org/10.1016/j.omtn.2023.01.004.

[8]Senior author

[9]These authors contributed equally

Correspondence: Ariadna Bargiela, Hospital Universitari i Politècnic La Fe, Valencia, Av. de Fernando Abril Martorell, 106, 46026 Valencia, Spain.
E-mail: ariadna_bargiela@iislafe.es

A

Loci	Cell line	
	Primary	Immortalized
D3S1358	17,18	17,18
TH01	7,7	7,7
D21S11	28,30	28,30
D18S51	13,15	13,15
Penta E	10,15	10,15
D5S818	10,11	10,11
D13S317	12,12	12,12
D7S820	10,11	10,11
D16S539	11,12	11,12
CSF1PO	10,10	10,10
Penta D	12,12	12,12
Amelogenin	X,Y	X,Y
vWA	16,18	16,18
D8S1179	14,15	14,15
TPOX	8,8	8,8
FGA	20.2,21	20.2,21

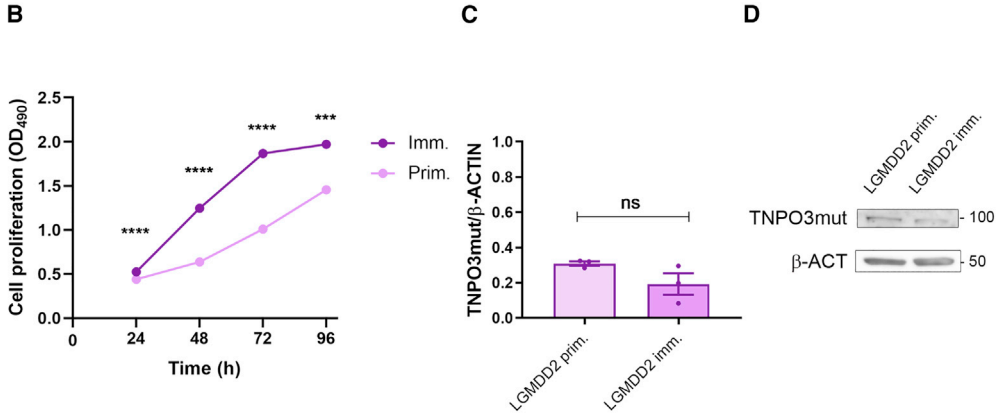

Figure 1. Validation of the immortalized myoblasts

(A) STR profiling of primary and immortalized LGMDD2 myoblasts. The numbers indicate the number of repeats per allele at the corresponding locus in the indicated cell lines. (B) Absorbance curves correspond to cell proliferation potential of primary and immortalized myoblasts. Asterisks denote significant differences in comparisons between both lines at each time point. (C and D) Quantification and representative blots of TNPO3 protein in primary and immortalized myoblasts obtained from a LGMDD2-affected donor. β-Actin was used as an endogenous control (n = 3). The bar graphs show the mean ± SEM; ns: non-significant, ***: $p < 0.001$, ****$p < 0.0001$, according to Student's t test.

reason why TNPO3mut leads to the clinical features of LGMDD2 is largely unknown.

LGMDD2 muscle biopsies have revealed a broad range of myopathic features, including p62 protein aggregates and increased LC3 signal, which indicates impaired autophagic activity.[2,12,13] Furthermore, increased autophagic flux was also reproduced by the LGMDD2 *Drosophila* model,[6] and chemical inhibition of the pathway with chloroquine (CQ) improved phenotypes.

Gene editing represents an exciting therapeutic strategy in inherited neuromuscular disorders.[14] Although the CRISPR-Cas9 system was initially described as a form of adaptive bacterial immunity,[15,16] some components of this natural system were adapted to enable gene editing in mammalian cells[17,18] and *in vivo*,[19] in virtually any organism. CRISPR can knock out genes of interest and induce precise changes in genomes. In this regard, homology direct repair (HDR) is helpful for point mutation correction or insertion of new DNA by inducing double-stranded breaks in the interest locus using CRISPR. In induced pluripotent stem cells derived from patients with limb-girdle muscular dystrophy types R2 and R3, CRISPR/HDR-mediated editing notably rescued protein expression.[20]

The lack of LGMDD2 models and therapeutic options prompted us to develop a patient-derived immortalized myoblast cell line and assess to what extent a gene-editing approach could rescue disease-associated phenotypes, including hyperactivated autophagy and terminal muscle differentiation markers. Our significant finding is that CRISPR-Cas9-mediated correction rescues up to 44% of the transcriptome changes associated with the disease, indicating that correction of the *c.2771delA* mutation in the *TNPO3* stop codon is a promising therapeutic approach for LGMDD2.

RESULTS

Generation of a LGMDD2 immortalized cell line from primary myoblasts

Because genetic editing of primary cells is inefficient due to technical complexity and low proliferative potential, we first immortalized primary LGMDD2 myoblasts by co-transducing them with *human telomerase reverse transcriptase* (*hTERT*) and *Cdk-4* transgenes.[21] Overexpression of these genes was confirmed in our RNA sequencing (RNA-seq) dataset compared with data from control (CNT) primary myoblasts available from independent experiments finding 184.13 and 182.89 transcripts per million (TPMs) in LGMDD2 immortalized myoblasts versus 6.47 and 0 TPMs in CNT primary myoblasts. Next, to unambiguously confirm the identity of the immortalized cells, we performed a short tandem repeat (STR) profiling, and both lines had the same 16 STRs in the analyzed loci (Figure 1A). The proliferation potential of these lines was analyzed at 24, 48, 72, and 96 h (Figure 1B) finding that the immortalized line proliferated significantly more than the primary line. To specifically quantify TNPO3mut, we developed a polyclonal antibody against the extra 15 aa causing LGMDD2 and confirmed similar TNPO3mut levels expression immortalized and primary myoblasts (Figures 1C and 1D).

Design and validation of CRISPR-Cas9-mediated targeting of *TNPO3* mutation

Bioinformatics tools[22] used to design CRISPR RNA (crRNA) predicted two potential off-targets in *HAS2-AS1* and *MBTPS1* genes, each with three mismatches (Table S1). We introduced the Cas9-single guide RNA (sgRNA) complex as ribonucleoprotein (RNP) because of its better cutting efficiency in hard-to-transfect cells (such as myoblasts) and fewer off-target effects than CRISPR plasmids.[23] Additionally, we introduced a single-stranded oligodeoxynucleotide (ssODN) as a template necessary for mutation correction by

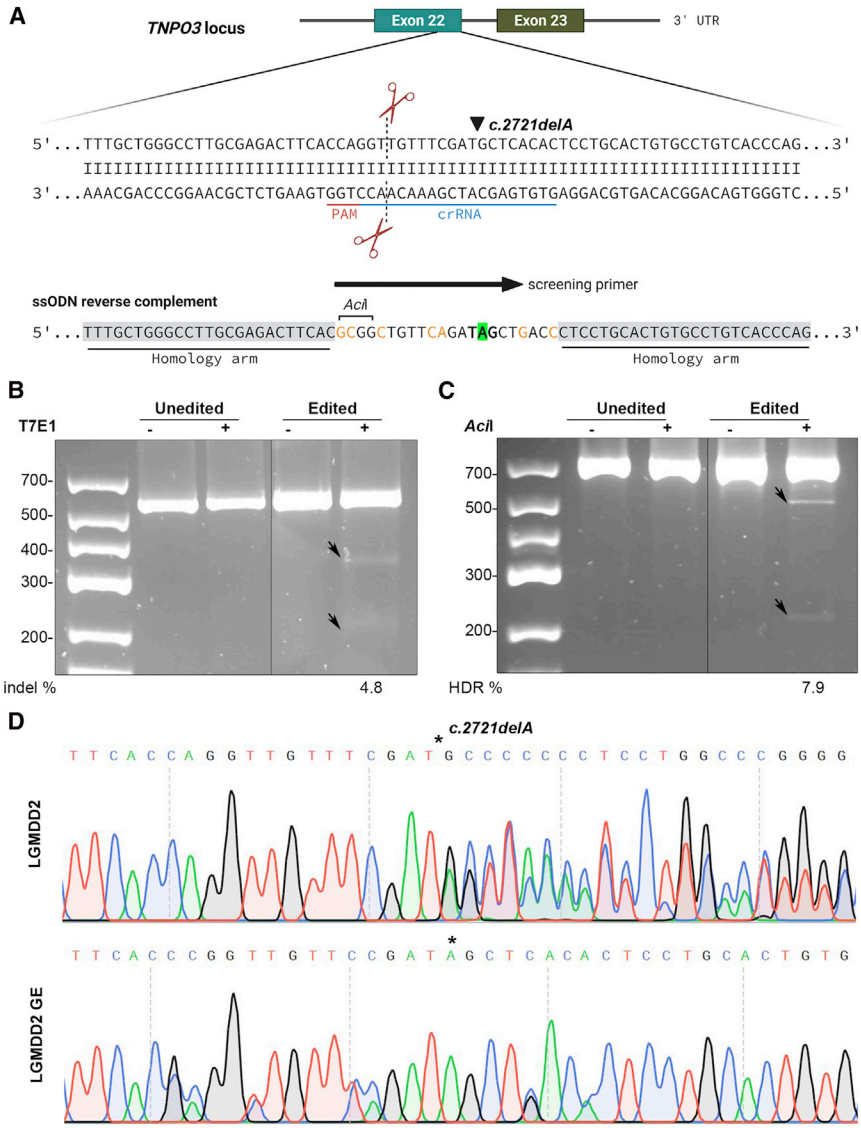

Figure 2. Correction of the *c.2771delA* mutation in LGMDD2 immortalized myoblasts

(A) Detail of the LGMDD2 allele (*c.2771delA*) in exon 22 of the *TNPO3* gene (created with BioRender.com). Blue lines indicate designed crispr RNA (crRNA), while red lines indicate its PAM sequence. The predicted Cas9 cleavage site (3 nt adjacent to the PAM sequence) is indicated by scissors and dotted line. The ssODN sequence was designed to repair the Cas9 DSBs by HDR, allowing the insertion of the missing adenine nucleotide (highlighted in green) and silent mutations (orange) to avoid Cas9 re-cutting. The ssODN sequence shown in (A) corresponds to the reverse complement of the ssODN that we used with the introduced changes; an *AciI* restriction site was created to quantify editing efficiency by RFLP assay. The arrow indicates the forward sequencing primer for PCR screening, and recombinant arms are marked in gray. (B and C) Agarose gel electrophoresis to visualize T7E1 cleavage products (arrows; B), corresponding to indel frequency, and *AciI* digestion products (arrows; RFLP assay; C) to evaluate editing efficiency. Both assays used DNA from edited and unedited cells without enzyme (–) as negative controls. The first lane corresponds to the molecular weight marker. (D) Sanger sequencing of the region encompassing the LGMDD2 mutation (upper panel) and confirmation of CRISPR-Cas9 gene editing (GE; lower panel). Double peaks in the LGMDD2 sample correspond to the superposition of wild-type and mutant allele sequences, while double peaks in LGMDD2 GE correspond to heterozygous silent mutations introduced with the ssODN. An asterisk in the upper panel denotes the missing adenine nucleotide, while in the lower panel it indicates their insertion, leading to restoration of the stop codon.

HDR (Figure 2A).[24–26] Cleavage efficiency by T7 Endonuclease 1 (T7E1) and editing efficiency by restriction fragment-length polymorphism (RFLP) assay were confirmed in gDNA (Figures 2B and 2C, respectively). The T7E1 assay showed an indel frequency of 4.8%, while the RFLP assay revealed an editing efficiency of 7.9%, indicating that Cas9-induced double-strand breaks were repaired using the ssODN as a template. However, the Tracking of Indels by Decomposition (TIDE) assay[27] estimated 87.4% indel frequency for the sgRNA. To reconcile these apparent discrepancies, we note that the T7E1 assay has been reported as inaccurate in genome-editing efficiencies higher than 30%.[28]

A plasmid expressing GFP was co-electroporated with RNP and ssODN into LGMDD2 myoblasts to facilitate GFP sorting by flow cytometry (fluorescence-activated cell sorting [FACS]). Single-cell colonies were amplified, and knockin events were evaluated in 81 clones by PCR. Twelve clones precisely incorporated the ssODN in the mutant allele, leading to the correction of the *c.2771delA* mutation and restoration of the stop codon. The silent mutations introduced are shown with double peaks in the Sanger electropherogram because of heterozygous incorporation of the ssODN (Figure 2D). Sanger sequencing confirmed that this patient exclusively carried the *c.2771delA* mutation in the *TNPO3* gene, thus discarding the other heterozygous mutations described in the gene leading to LGMDD2.[3–5,7,29] Seven clones were selected for further characterization, and predicted off-targets were evaluated by Sanger sequencing, in which no alterations were detected (Figure S1).

CRISPR-Cas9 editing of *TNPO3* mutation restores expression of disease-related genes (DRGs) and microRNAs (miRNAs)

The impact of the LGMDD2 mutation and CRISPR correction in *in vitro* myotubes was addressed at the transcriptome level. We obtained reads for 16,300 genes (Table S2), of which 2,508 (15%) were differentially expressed between healthy CNT and LGMDD2 myotubes (LGMDD2) and were considered DRGs. We observed a

homogeneous distribution between down- and up-regulated gene expression (1,236 and 1,272, respectively) (Figure 3A). Moreover, DRG expression was analyzed in LGMDD2 muscle cells that underwent CRISPR-Cas9 genome editing (LGMDD2 GE) and classified into four categories: (1) genes that did not significantly change on treatment (unrecovered), (2) genes that recovered between 10% and 50% of normal expression (partially recovered), (3) genes that recovered between 50% and 150% of normal expression (totally recovered), and (4) genes that changed above 150% of normal expression (over-recovered). We found that 44% of DRGs were significantly recovered with CRISPR editing (729 partially, 344 totally, and 37 over-recovered; Figure 3B). Subsequently, we focused on the 29% totally recovered genes (Figure 3C). Unsupervised clustering by Euclidean distance showed that most DRGs rescued by CRISPR editing were over-expressed in disease cells. Additionally, as the dendrogram shows, the expression profile of edited cells was closer to healthy CNT myotubes than to LGMDD2. Finally, we performed an over-representation analysis (ORA; $p < 0.05$) considering the Gene Ontology (GO) pathways. By comparing CNT versus LGMDD2, CNT versus LGMDD2 GE, and LGMDD2 versus LGMDD2 GE, we identified pathways altered by the disease (Disease), pathways that approached normal expression on GE (Treatment), and pathways responsive to the manipulation (Specificity), respectively (Figure S2). Of particular interest were that Wnt and BMP signaling pathways recovered CNT-type expression patterns, and the effect was specific as alterations decreased on GE compared with untreated LGMDD2 (Figure 3D). These pathways have pleiotropic effects in normal and disease muscle physiology[30] and constitute prime targets for a mechanistic understanding of disease pathogenesis.

Because most of the transcriptome did not recover normal levels on GE, including some GO pathways (Figure S3), and considering the relevance of miRNAs in the pathogenic mechanism of other myopathies,[31–33] we hypothesized that miRNA alterations might remain after the manipulation and contribute to gene expression changes after the originating mutation has been reverted. To this end, we performed an small RNA (sRNA) sequencing and analyzed miRNAs expression. Then, we identified 764 miRNAs in the CNT versus LGMDD2 comparison, of which 214 were differentially expressed (28%) (Table S2). Of those, around 49% were recovered in the GE line, whereas 50% remained unchanged, and the remaining 1% of miRNAs were over-recovered (Figures 3E and 3F). Thus, a significant percentage of miRNome changes was refractory to GE rescue, supporting the possibility of contributing to the transcriptome ones.

Proliferation potential and TNPO3 expression are restored to basal levels in CRISPR-Cas9-corrected cells

Because we detected a significant difference in proliferation potential between CNT and LGMDD2 myoblasts, we quantified this cell phenotype by 3-(4,5-dimethylthiazol-2-yl)-5-(3-carboxymethoxyphenyl)-2-(4-sulfophenyl)-2H-tetrazolium (MTS) assay in GE cells to assess rescue (Figure 4A). Results confirmed a significant increase of proliferation in the model cells at all times, and a reduction on CRISPR-Cas9 editing at 24, 48 and 72 h that was validated in six additional GE lines (Figure S4).

Previous studies demonstrated that TNPO3 protein was strongly upregulated in skeletal muscle biopsies from LGMDD2 patients and in somatic musculature and motor neurons in the *Drosophila* model.[4,6] Similarly, we quantified TNPO3 expression at the transcript and protein levels in CNT, disease, and CRISPR-edited cells at 0, 4, and 7 days of differentiation (Figures 4B–4D). In CNT cells, *TNPO3* transcripts increased as cells differentiated into myotubes, reaching almost 2-fold expression at day 7 versus day 0 ($p = 0.0071$; Figure 4B). This effect was not as evident for protein, although a trend was observed (Figure 4C). In LGMDD2 myotubes, we quantified strong TNPO3 overexpression in mRNA and protein, ranging from 1.5- to 3-fold compared with CNT counterparts, respectively. Moreover, in CRISPR-corrected cells, TNPO3 levels dropped to levels like CNT myotubes in all evaluated conditions.

In western blot, the antibody was specific for TNPO3mut because no signal was detected in CNT or CRISPR-edited cells (Figure 4E). Furthermore, TNPO3mut expression levels did not significantly change throughout myotube differentiation (Figure 4F). Importantly, a similar trend to reduce total and mutant TNPO3 protein levels on mutation edition was detected in six additional CRISPR-corrected clones (Figure S4).

Differences have been previously reported between CNT and patient biopsies in the subcellular localization of TNPO3.[12] To assess this phenotype in the cell model, we immunodetected total TNPO3 (mutant and wild type) at 0 and 7 days of differentiation (Figures 4G–4L). We observed nuclear and cytoplasmic punctate signals in CNT and model cells at both differentiation times, but these were weaker in disease cells. On correction of the mutation, the TNPO3 pattern shifted toward a CNT-like one.

Considering TNPO3 involvement in alternative splicing regulation[8] and similarities in phenotypes related to muscle weakness and atrophy between myotonic dystrophy type 1 (DM1) and LGMDD2,[34] we investigated the inclusion of exon 10 in pyruvate kinase M transcripts (PKM2; embryonic M2 isoform). PKM2 is specifically induced in DM1 patients and has been suggested to affect metabolic homeostasis and cause energy deficits associated with muscle weakness and wasting.[35] Notably, the PKM2 isoform was significantly increased in LGMDD2 model myotubes (20% increase), and this mis-splicing was restored toward a CNT-like pattern on mutation editing.

CRISPR-Cas9 gene editing rescues muscle cell differentiation defects caused by the LGMDD2 mutation

Impaired muscle differentiation has been reported in other limb-girdle muscular dystrophies and neuromuscular disorders[36–38] and as a role for TNPO3.[11] To address changes in myoblast fusion and myotube diameter associated with LGMDD2, we performed immunostaining of Desmin, a muscle-specific type III intermediate

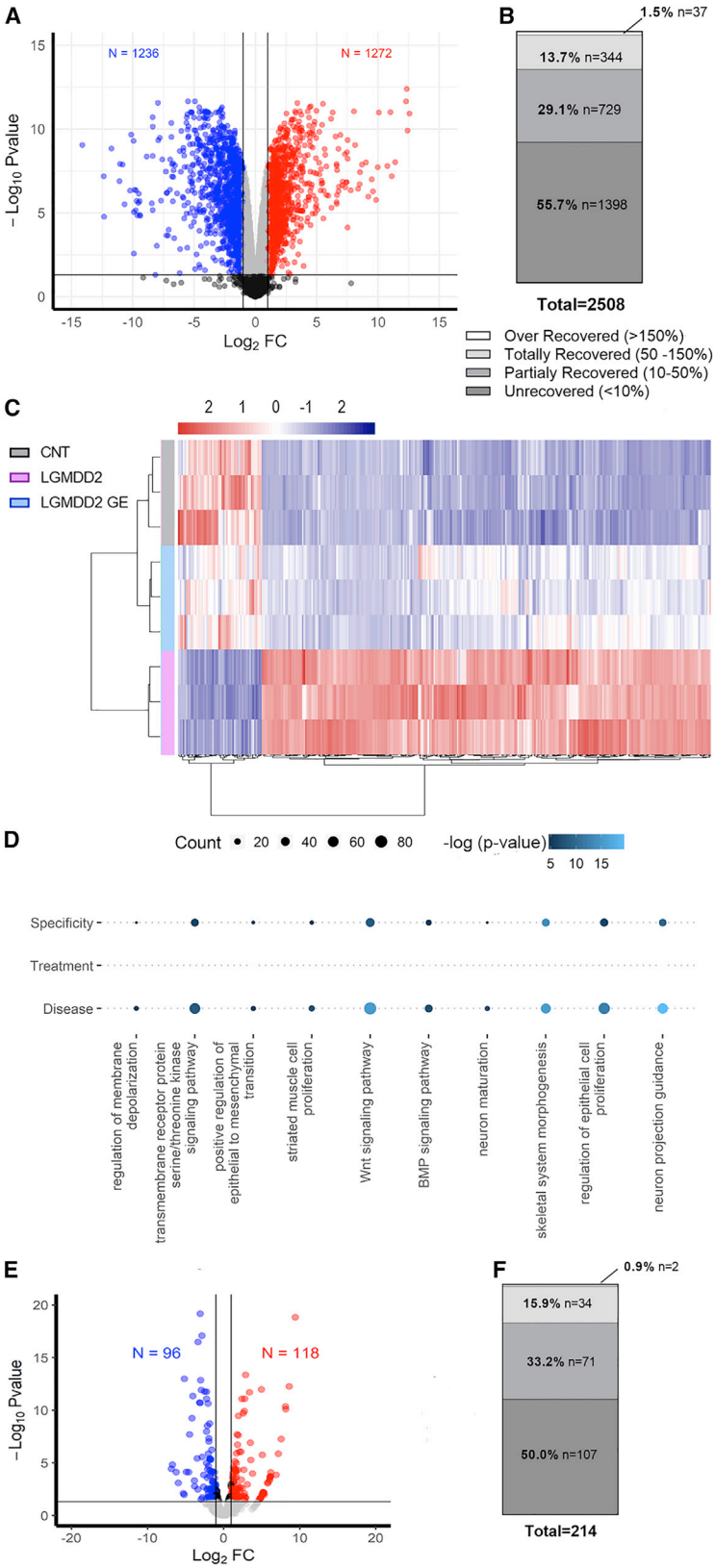

Figure 3. Myotube transcriptome changes in LGMDD2 cells are significantly rescued on CRISPR-Cas9 editing

(A) Volcano plot that represents differentially expressed genes between healthy control and LGMDD2 myotubes. Black lines indicate $|\log_2 FC| = 1$ in x axis and $-\log_{10}$ P-value = 1.3 in y axis, which are the fold change (FC) and significance (P value) thresholds for significantly differentially expressed genes. Dots represent downregulated (blue) or upregulated (red) genes. (B) Percentage of genes differentially expressed between CNT and LGMDD2 cells (regarded as disease-related genes [DRGs]; 2,508), whose expression did not significantly approach that in normal cells (unrecovered), partially recovered, totally recovered, or departed > 150% from normal values (over-recovered) after CRISPR editing of the mutant TNPO3. (C) Heatmap of the 729 DRGs that were totally recovered by CRISPR-Cas9 edition in our dataset of healthy (CNT), model (LGMDD2), or edited (LGMDD2 GE) cells. Differences were assigned a color according to the scale: red = over-expressed; blue = under-expressed. (D) Representation of significantly recovered pathways in the indicated conditions. Each point represents a significant over-represented pathway, and each column is a different comparison: Disease (CNT versus LGMDD2), Treatment (CNT versus LGMDD2 GE), and Specificity (in LGMDD2 versus LGMDD2 GE). Size represents the count of altered genes in each over-represented pathway, while the color denotes the significance of each over-representation in that pathway. Significant recovery involves that the Treatment comparison is no longer significantly enriched (hence lack of dots) and both Disease and Specificity comparisons are significantly enriched. (E) Volcano plot uses the same conventions as in (A) and represents differentially expressed miRNAs between healthy control and LGMDD2 myotubes. (F) Percentage of miRNAs unrecovered, partially recovered, totally recovered, or over-recovered after CRISPR editing of the mutant TNPO3.

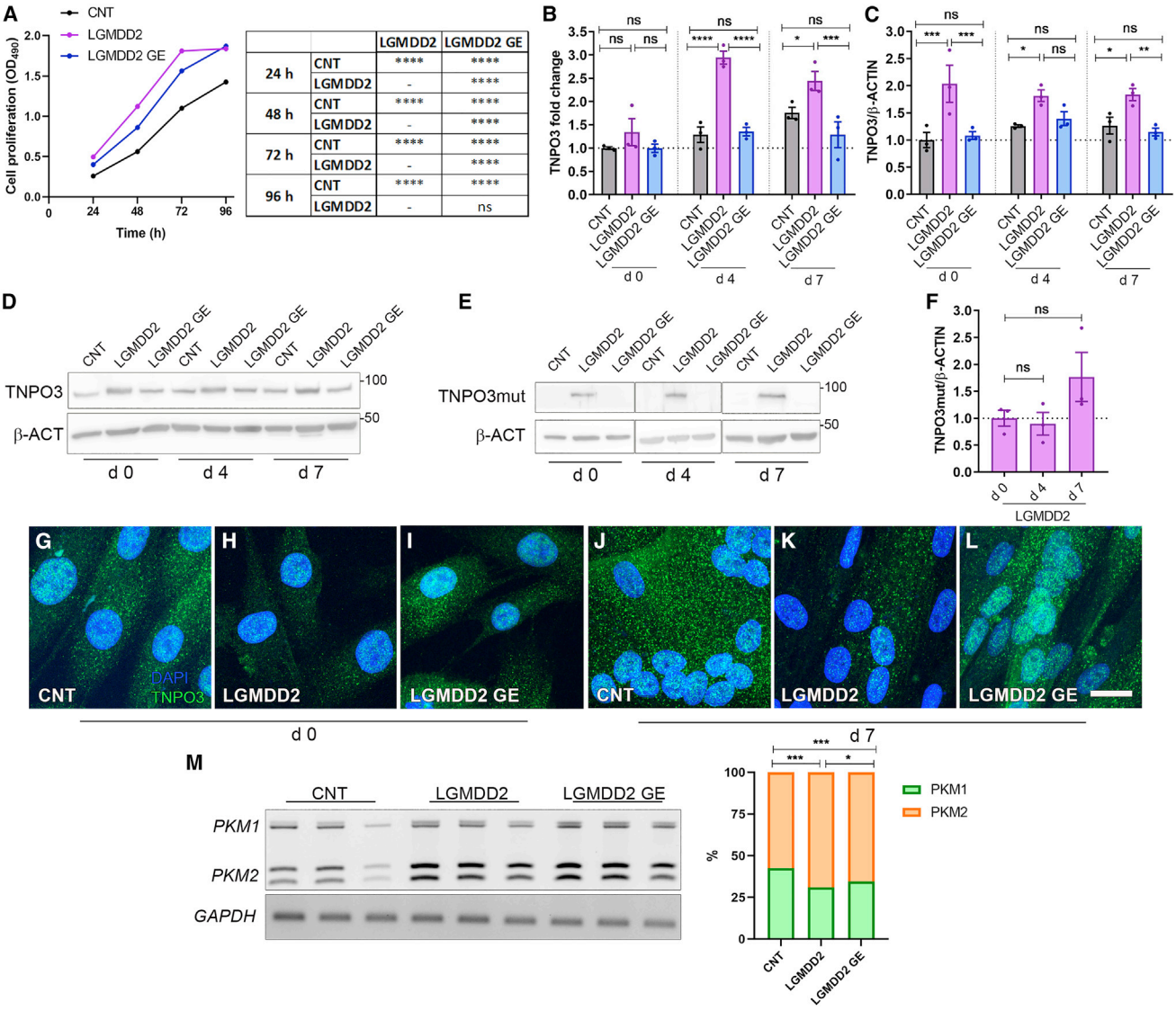

		LGMDD2	LGMDD2 GE
24 h	CNT	****	****
	LGMDD2	-	****
48 h	CNT	****	****
	LGMDD2	-	****
72 h	CNT	****	****
	LGMDD2	-	****
96 h	CNT	****	****
	LGMDD2	-	ns

Figure 4. Impaired TNPO3 phenotypes are restored in CRISPR-Cas9-corrected cells

(A) Absorbance curves representing cell proliferation potential of control (CNT; gray), LGMDD2 (LGMDD2; purple), and CRISPR-Cas9-edited cells (LGMDD2 GE; blue) measured at the indicated time points. (B) TNPO3 quantification by qRT-PCR, relative to the mean of *GAPDH*, *GPI*, and *HPRT1* expression levels, in the indicated cell lines differentiated for 0, 4, and 7 days. All values were normalized to the CNT condition at day 0 (dashed line) (n = 3). (C and D) Quantification and representative blots of TNPO3 immunodetection. β-Actin was used as an endogenous control to normalize TNPO3 protein levels (n = 3). (E) Representative blots of immunodetection of mutant TNPO3 in the same conditions described in (A). (F) Quantification of the mutant TNPO signal in a cell model from blots shown in (D) (n = 3). Values were normalized to the signal detected in LGMDD2 cells at day 0 of differentiation. (G–I). Representative confocal images of TNPO3 immunodetection (green) in control, LGMDD2, and LGMDD2 GE myoblasts at day 0 (G–I, respectively), and the same lines differentiated for 7 days (J–L). Nuclei were stained with DAPI. Scale bar: 20 μm. (M) Agarose gels of semiquantitative RT-PCR analyses of PKM isoforms, and percent of *PKM1* and *PKM2* RNA isoforms in the indicated cells. The bar graphs show the mean ± SEM; ns: non-significant, *: $p < 0.05$, **: $p < 0.01$, ***: $p < 0.001$, ****: $p < 0.0001$, according to the one-way ANOVA test.

filament essential for proper muscular structure and function, to quantify fusion capacity and myotube diameter (Figures 5A–5F). Undifferentiated cell staining showed no differences between the lines, because no fusion was detected. In 7-day differentiated LGMDD2 myotubes, both parameters were significantly reduced by around half compared with CNTs, while CRISPR-corrected cells partially recovered fusion index and diameter (Figures 5G and 5H, respectively). We also performed myosin heavy chain (MHC) immunostaining in the same cells (Figures 5I–5L) as a marker of late differentiation of myotubes.[39] Our analyses confirmed impaired terminal muscle differentiation of LGMDD2 cells, in which less than 10% of the nuclei corresponded to MHC$^+$ cells, compared with

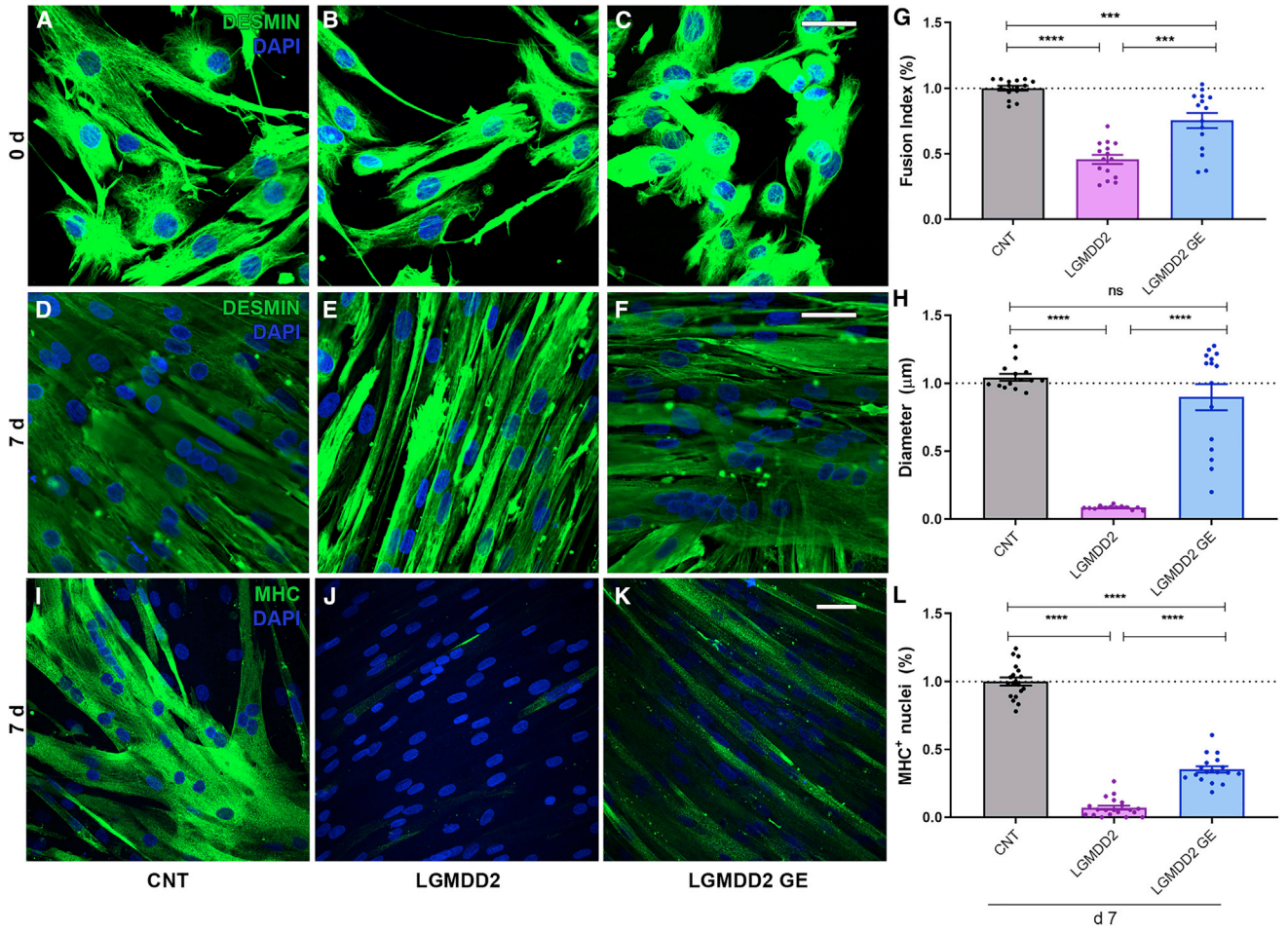

Figure 5. Defects in differentiated muscle markers in LGMDD2 improved in CRISPR-Cas9-edited cells

(A–F) Representative confocal images of Desmin immunofluorescence (green) in control (CNT; A and D), disease model (LGMDD2; B and E), and CRISPR-Cas9-edited (LGMDD2 GE; C and F) myoblasts at day 0 (A–C) and day 7 (D–F) of differentiation. (G and H) Quantification of the myogenic fusion index and myotube size of the cell lines indicated in (D)–(F). (I–K) Representative confocal micrographs of MHC immunostaining (green) in control, disease model, and CRISPR-edited myotubes at day 7 of differentiation. (L) Quantification of the percentage of nuclei within MHC^+ cells in each condition. Nuclei were stained with DAPI. Scale bars: 40 µm (both immunodetections). All data were normalized to the CNT condition. The bar graphs show the mean ± SEM; ns: non-significant, ***: $p < 0.001$, ****: $p < 0.0001$, according to the one-way ANOVA test.

65% in CNT myotubes. Similar to fusion index and diameter, CRISPR editing of the mutation was sufficient to improve this phenotype significantly, showing double the number of nuclei inside MHC^+ myotubes than in diseased cultures. Alike results were obtained with additional edited clones (Figure S5).

Elevated autophagic activity induced by TNPO3 mutation is restored on CRISPR-Cas9 editing

We previously reported hyperactivation of autophagy in an LGMDD2 *Drosophila* model of disease[6] consistently with abnormal patterns in autophagy markers in human muscle samples.[13] Here, we investigated autophagy status by immunofluorescent detection of LC3-I and LC3-II (Figures 6A–6D). A clear and more intense dotted pattern was detected in model myotubes compared with healthy CNTs. The punctate pattern corresponds to LC3 conjugated to membrane-bound phosphatidylethanolamine (LC3-II) in autophagosomes.[40] In CRISPR-corrected cells, in contrast, the signal reverted to that observed in CNTs and became predominantly cytoplasmic and diffuse, indicating the presence of soluble LC3-I, and consequently reduced autophagic levels. Quantification of the number of dots per unit of cell area confirmed a significant 2-fold increase in model myoblasts and reduction in CRISPR-corrected cells (Figure 6D). Additionally, cells were dyed with LysoTracker, an acidotropic dye that marks the acidic cellular compartments as lysosomes and autophagolysosomes, confirming increased activity of the catabolic pathway in LGMDD2 and rescue in GE myotubes (Figures 6E–6G).

Autophagy activation by TNPO3mut was finally assessed at the protein level (Figures 6H and 6I). We analyzed levels of ATG7, which

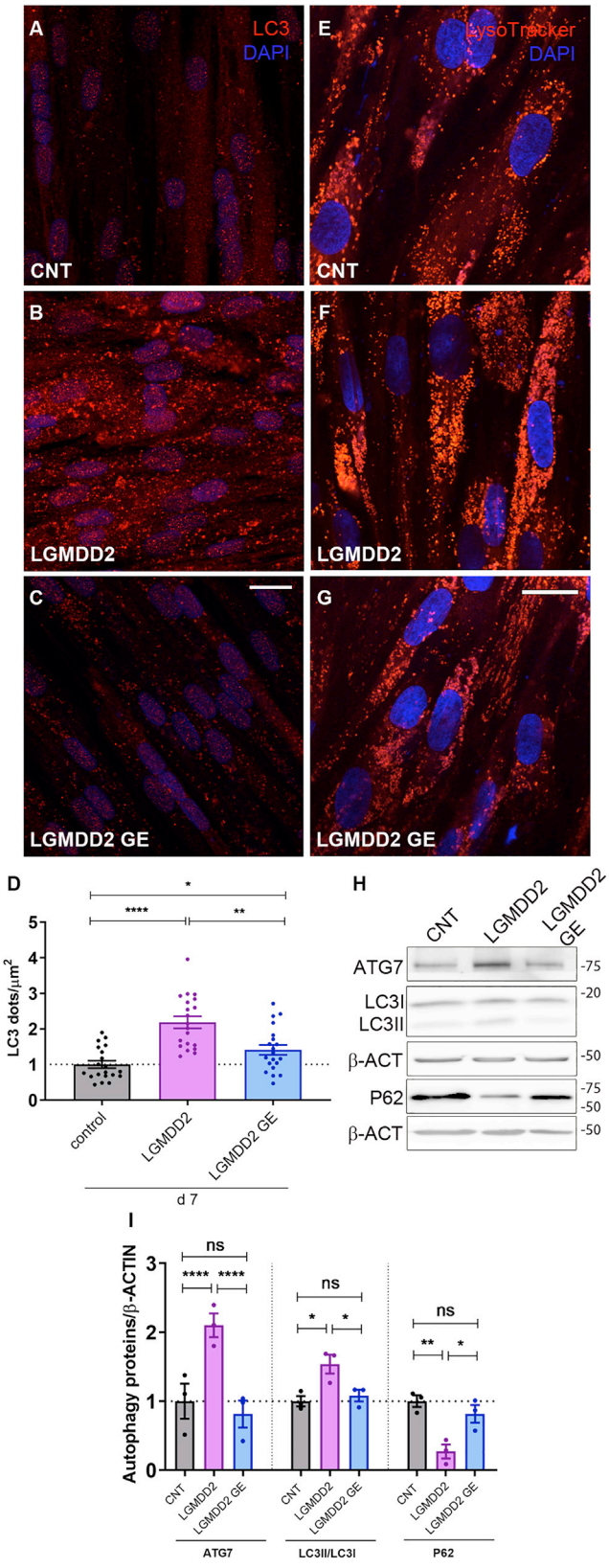

Figure 6. Overactivation of autophagy in LGMDD2 myotubes is restored on CRISPR editing of the mutation

(A–C) Confocal images of LC3 immunofluorescence (red) or (E–G) LysoTracker staining (red) in 7-day-differentiated myotubes of the control (CNT; A and E), disease model (LGMDD2; B and F) and CRISPR-Cas9-edited (LGMDD2 GE; C and G) myotubes. Nuclei were stained with DAPI. Scale bars: 20 µm. (D) Quantification of LC3 puncta per square micrometer in each condition shown in (A)–(C). (H and I) Representative western blots (H), with indication of molecular weight sizes to the right in kDa and quantification (I) of total ATG7 protein, the LC3-II/LC3-I ratio, and P62 in protein extracts from healthy control (CNT), LGMDD2, and edited LGMDD2 cells differentiated for 7 days (n = 3). β-Actin was used as an endogenous control. All data were normalized to the CNT condition (black dashed line). The bar graphs show the mean ± SEM; ns: non-significant, *: $p < 0.05$, **: $p < 0.01$, ****: $p < 0.0001$, according to the one-way ANOVA test.

promotes phagophore growth by means of ATG8 lipidation through its E1-like enzymatic activity.[41] We observed a 2-fold increase in diseased cells compared with healthy CNTs. We analyzed autophagic flux by means of autophagosome-associated and soluble LC3 (LC3II/LC3I ratio). Results denoted pathological activation of autophagic flux in LGMDD2 cells and restoration with CRISPR correction. This was also confirmed in six additional edited clones (Figure S6). Finally, we assessed flux activation by the quantification of levels of P62, a scaffold protein that carries cargoes committed to lysosomal degradation to the autophagosome. P62 is removed by autophagic activity.[42,43] Confirming overactivation, we detected an approximately 3-fold reduction in model cells, while P62 levels in CRISPR-corrected cells were like healthy CNT myotubes.

To provide further evidence of increased autophagic flux, we used expression vectors of both mCherry-GFP-tagged LC3 and P62 proteins. In brief, the GFP signal from these fusion proteins is quenched in an acidic environment, whereas mCherry remains.[44] Transfection of mCherry-GFP-LC3 denoted a dominant mCherry signal in LGMDD2 compared with CNT, thus supporting an increased autophagic flux in the disease model (Figures 7A and 7B). GE increased the GFP signal similar to that of mCherry, indicating relief of excessive autophagic flux from model myotubes (Figure 7C). Besides, LGMDD2 cells were treated with autophagic inhibitor CQ, as a CNT, and the signal was like that observed in edited cells (Figure 7D). Similar results were obtained when myoblasts were transfected with mCherry-GFP-P62 (Figures 7E–7H). These data support the hypothesis that *TNPO3* editing is sufficient to restore autophagic status in LGMDD2 myotubes.

DISCUSSION

As already shown in LGMDD2 biopsy studies, immunodetection of total TNPO3 confirms its accumulation in patient cells.[4] We further found this accumulation to be mutation dependent because, after mutation editing, levels were similar to those from healthy CNTs. However, immunofluorescence of TNPO3 suggests the opposite, with a weaker signal in model myoblasts and signal recovery after GE; these results agree with previous experiments on patient biopsies reporting a milder signal using two different antibodies against TNPO3.[12] Larue

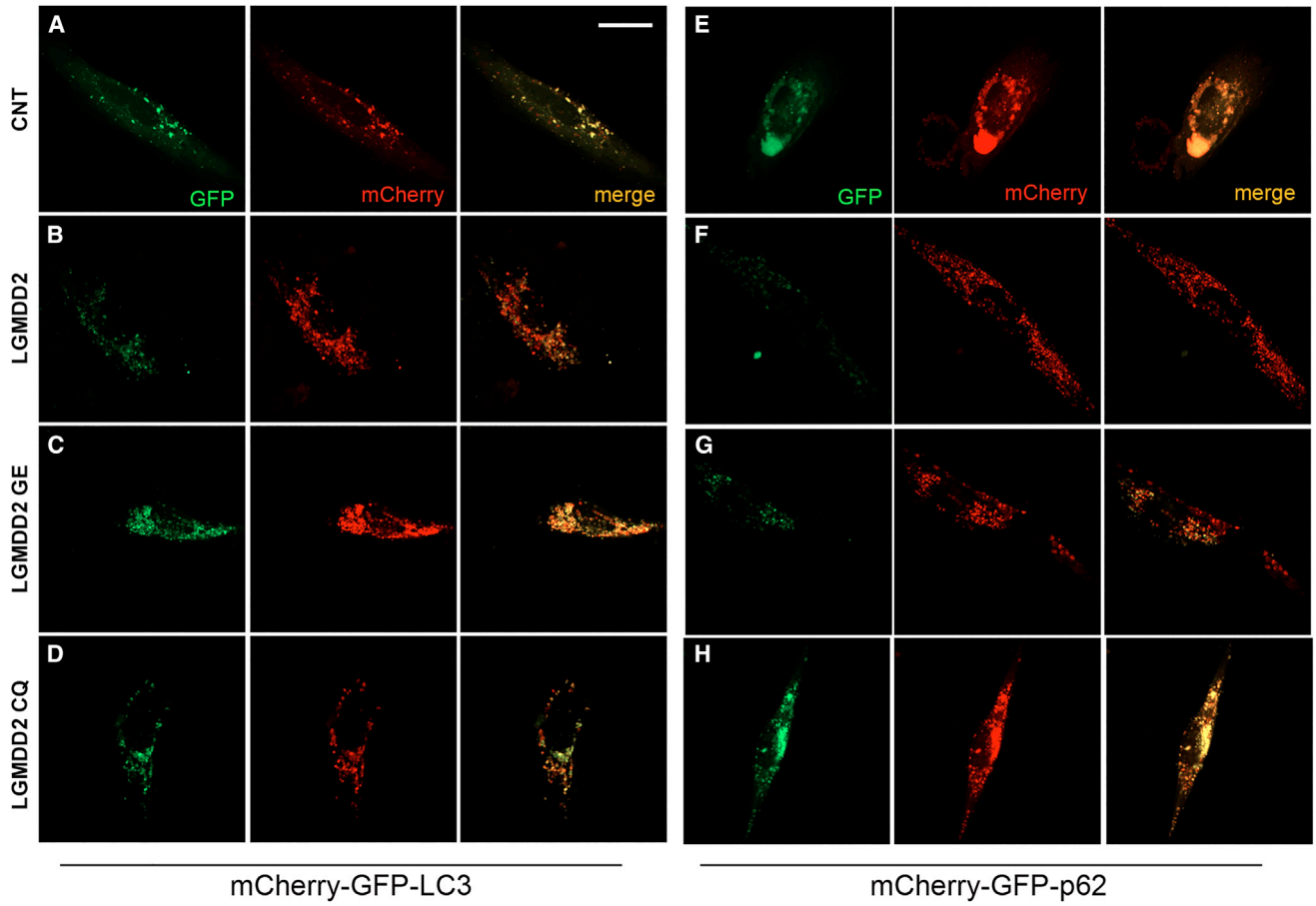

Figure 7. Autophagic flux is reverted by mutation restoration

Representative confocal images of fluorescent LC3 (A–D) or p62 (E–H) puncta. CNT, LGMDD2, and LGMDD2 GE myoblasts were transfected with mCherry-GFP-LC3 (A–C) or mCherry-GFP-p62 (E–G) plasmids. Disease model cells were also treated with 10 μM chloroquine for 16 h as a positive control of autophagy blockade (D and H). The merged images (yellow) show overlap of GFP (green) and mCherry (red). Scale bar: 20 μm.

et al.[45] described the capacity of TNPO3 dimerization, specifically under high protein concentrations. In an LGMDD2 context, there exists the possibility of heterodimers formation because of the presence of the wild-type and mutated forms.[46] Then, probably under native conditions, the immunogenic region is not accessible for the antibody in the heterodimeric conformation, thus showing a milder signal. Therefore, whereas by western blotting the antibody would simultaneously detect TNPO3wt and TNPO3mut, immunofluorescence would detect only the wild type, half of which is expressed by patients because it is an autosomal dominant disease. Indeed, heterodimers could act as transdominant negatives, possibly interfering with the TNPO3 function. Besides, the extra 15 aa could give greater stability to the heterodimer and consequently contribute to its accumulation; however, available bioinformatics tools do not predict any specific role for the 15 extra amino acids in TNPO3mut.[47]

TNPO3 imports SR proteins, which are regulators of alternative splicing and mRNA metabolism, and transports them to the nucleus.[8,48] Proper muscle functioning and development is at least partially determined by its specific proteome, determined by alternative splicing.[49] In fact, defects in the regulation of alternative splicing cause several symptoms in other neuromuscular diseases such as DM1.[50] Here we have demonstrated altered splicing in LGMDD2, specifically a mis-splicing of PKM, which in DM1 has been proposed to contribute to the atrophy phenotypes of the disease.[35] Significantly, SRSF10 protein, transported to the nucleus by TNPO3, regulates alternative splicing of *Lrrfip1*, and its correct use of alternative exons in skeletal muscle is essential for myoblast differentiation.[51] Similarly, SRSF1 inhibits autophagy by regulating Bcl-x splicing.[52] Thus, defects in exon use regulation may also contribute to LGMDD2 pathology. This could, in turn, lead to defects in differentiation in LGMDD2 myotubes, which expressed fewer MHCs than CNTs and had impaired fusion capacity and diameter. Indeed, both alterations are ultimately caused by TNPO3mut toxicity because the phenotypes reverted to non-pathological parameters on CRISPR-editing removal.

Autophagy alteration has been identified in patient biopsies and in a *Drosophila* model,[6,13] and the immortalized LGMDD2 muscle cells

reported in this work also reproduce this phenotype. In other neuromuscular diseases, including other limb-girdle muscular dystrophies, autophagy overactivation is one of the triggers leading to muscle wasting.[53–55] Moreover, in DM1 and Pompe disease, inhibition of autophagic activity showed a beneficial effect in animal models.[56–58] There is currently no available treatment for LGMDD2, but GE seems a valid approach given that it is a monogenic disease. In 2020 there were almost 20 registered interventional clinical trials with CRISPR-based gene editing, focused on cancer treatment[59] but also in Duchenne muscular dystrophy with trials designed to edit the mutated *dystrophin*.[60] *In vivo* therapeutic approaches have also been performed in other neuromuscular disorders, specifically in mice for congenital muscular dystrophy 1A and DM1.[61,62] Here, we report a proof of concept of the suitability of GE using CRISPR-Cas9 in the context of LGMDD2 wherein 44% of DRGs were significantly recovered after mutation editing. Nevertheless, it cannot be ruled out that a small subset of the genes corrected after CRISPR-Cas9 editing may have done so because of the genetic manipulation and not the correction of the mutation. Additionally, CRISPR editing has a specific effect on cell signaling as transmembrane receptor protein serine/threonine kinase and Wnt pathway. These data offer new lines of study in the disease's pathogenesis mechanism.

The GO database has not identified autophagy as a pathway differentially activated in model cells. However, we confirmed its overactivation by complementary approaches, including protein quantification and activity markers. These data exemplify that information obtained by transcriptome analysis is significantly different from that gathered by other protein-based techniques, such as mRNA and protein amounts, are only modestly correlated quantitatively, indicating strong post-transcriptional regulation in controlling gene expression.[63]

The rescue of differential expression in the edited cells was partial, and not all DRGs were recovered. Similarly, in other myopathies where CRISPR-Cas9 editing was used to correct a single mutation, such as DM1, pathological phenotypes, including ribonuclear foci or alternative splicing of *SERCA*, were not completely reversed after the removal of the mutation.[64] Indeed, there may be factors contributing to disease pathogenesis besides TNPO3mut, such as miRNA alterations that, once triggered, are maintained independently of the mutation through autoregulatory loops. miRNAs are relevant to pathological phenotypes in the most common skeletal muscle dystrophies, including Duchenne and Becker, DM1 and spinal muscular atrophy, among others.[65,66] Supporting this, about 50% of the miRNAs associated with LGMDD2 remained unchanged after correcting the mutation, thus maintaining cascading effects on their corresponding mRNA targets.

The LGMDD2 *Drosophila* model entails a series of limitations, because it is an invertebrate organism and most biomedical researchers lack the facilities and experience for its use. To overcome these issues, here we describe an immortalized muscular cell model that is a tool for studying pathogenesis mechanisms, identifying therapeutic targets, and drug screening. This model accurately reproduces relevant phenotypes of the disease and provides the basis for a proof of concept that CRISPR-Cas9 editing is a suitable therapeutic approach for LGMDD2.

MATERIALS AND METHODS

CRISPR-Cas9 design

A 20-nt crRNA was designed using the Breaking-Cas bioinformatics tool[22] (that evaluates the potential off-targets) to target the mutated allele, and its expected cleavage site was close to the *c.2771delA*, conferring more specificity over this allele than the wild type. The ssODN template for HDR was designed to contain 60-nt homology arms identical to the non-targeting strand, defined as the genomic strand containing the protospacer adjacent motif (PAM), flanking the sequence to introduce (5′-AGTCCGGACAAAAGCTGGGAAC TATGTATCCTCACCTGGGTGACAGGCACAGTGCAGGAGGGT CAGCTATCTGAACAGCCGCGTGAAGTCTCGCAAGGCCCAGC AAACTTGTTTACATTCCTCAGCACTAGAAAAGAAAAGG-3′). The knockin sequence contains the A nucleotide missing in one allele of the LGMDD2 cells, as well as silent nucleotide changes in the sgRNA and PAM sequence to prevent Cas9 from reiterated cleavage after HDR. An *Aci*I restriction enzyme site was also introduced for the RFLP assay and for designing a specific primer (Table S1) to screen the clones. The ssODN was synthesized by Ultramer Oligonucleotides (Integrated DNA Technologies).

Cleavage and gene-editing testing

The CRISPR-Cas9 components were introduced as RNP. The crRNA, complementary to the target locus, and the trans-activating CRISPR RNA (tracrRNA), that binds the crRNA to the Cas9 protein, were hybridized to form the sgRNA by 5 min of incubation at 95°C. The RNP complex was formed by mixing 104 pmol purified *S. pyogenes* Cas9 nuclease with 120 pmol of the sgRNA duplex (Integrated DNA Technologies).

For RNP complex delivery, 2×10^5 LGMDD2 immortalized myoblasts were resuspended in 20 μL of P5 nucleofector solution with 110 pmol electroporation enhancer and 120 pmol of the ssODN and were electroporated with the Amaxa 4D-Nucleofector using the EY-100 program and 16-well Nucleocuvette Strips (Lonza, Basel, Switzerland).

T7E1 and RFLP assays were performed to evaluate cleavage and editing efficiency 48 h after RNP and RNP + ssODN electroporation, respectively. Genomic DNA was amplified with primers targeting the cleavage site (Table S1), and the PCR products were purified. T7E1 assay was performed, and indel frequencies were calculated as previously described.[67] For the RFLP assay, 300 ng of purified DNA PCR product was incubated with the *Aci*I restriction enzyme (ThermoFisher Scientific, Waltham, MA, USA), following the manufacturer's protocol. Digested products were resolved on 2% agarose gel, and band intensities were measured with the ImageJ software (NIH).[68]

Cleavage efficiency was also calculated using the TIDE assay.[27] In our case, the untreated LGMDD2 cell sample shows double peaks from the mutation point downstream because of the heterozygous *c.2771delA* in the Sanger chromatogram (Figure 2D). This region overlaps with the sgRNA sequence, and the TIDE program did not predict any cleavage site. The treated sample (DNA from LGMDD2 cells electroporated with the RNP) showed fewer double peaks because of the introduction of indels that partially restored the reading frame. To address this issue, we used the treated sample chromatogram as a CNT sample and the untreated chromatogram for the test sample. For the sgRNA sequence, we used an adjacent sequence without overlapping double peaks (without affecting the results because the cleavage efficiency is calculated within a window of 100 bp). A heterozygous mutation (X and Y alleles) edited with 100% efficiency, in the Sanger traces, will show 50% X/50% Y signal going to 100% X and 0% Y. "Fooling" TIDE uploading the treated sample as CNT and vice versa in the 100% efficient case X would turn to X/Y. Because only 50% of the DNA was modified, because there was only one allele to edit, cleavage efficiency was $100 - (50\% - X\%) \times 2$. In our case, we obtained a 43.7% X allele. Therefore, if 50% X = 100% efficiency, then 43.7% X = 87.4% efficiency.

Generation of edited clones

To generate edited clones with the *c.2771delA* corrected by HDR, we electroporated 2×10^5 LGMDD2 immortalized myoblasts with RNP and ssODN as described earlier together with 1 μg of the pmaxTMGFP vector (Lonza). At 48 h after electroporation, myoblasts were trypsinized and collected in sorting buffer (HEPES 25 mM, EDTA 5 mM, BSA 1% in PBS) for single-cell FACS in a FACSAria-III sorter (Becton Dickinson). The GFP-positive cells were seeded individually in 96-well plates and amplified to form homogeneous single-cell colonies, as previously described.[69] DNA was extracted from the successfully grown clones and analyzed by PCR with the screening primer designed in the ssODN. PCR products were resolved in a 1% agarose gel, and positive colonies were Sanger sequenced to confirm that the ssODN was introduced correctly. One edited clone was amplified for further functional characterization, and we analyzed the two potential off-targets by Sanger sequencing.

Cell culture conditions and myoblast immortalization

Muscle biopsies to obtain primary myoblasts were taken from the tibialis anterior of a 33-year-old male LGMDD2 donor, after informed consent, in La Fe University Hospital (Valencia, Spain; research ethics committee authorization 2016/0388), as previously described.[70] CNT myoblasts were provided by the Institute of Myology biobank, Paris (ID AB1079) and were obtained from the quadriceps of a 38-year-old healthy male donor.

Human primary myoblasts were transduced with both hTERT and Cdk-4 lentiviral vectors with a ratio of number of transducing lentiviral particles to number of cells (MOI) of 5 in the presence of 4 μg/mL polybrene (Sigma-Aldrich, Saint Louis, MO, USA). Transduced cell cultures were selected with puromycin (0.2 μg/mL; Life Technologies, Carlsbad, CA, USA) for 4 days and neomycin (0.3 mg/mL; Life Technologies) for 10 days. Cells were seeded at clonal density, and selected clones were isolated from each population using glass cylinders.[21]

Immortalized myoblasts were cultured with Skeletal Muscle Cell Growth Medium (PELOBiotech, Planegg, Germany). Differentiation medium, when needed, was prepared with Dulbecco's modified Eagle's medium high-glucose, 2% horse serum, and 1% penicillin and streptomycin (ThermoFisher Scientific). Cells were grown at 37 °C in a humidified atmosphere containing 5% CO_2.

Generation of an anti-TNPO3mut antibody

A TNPO3mut-specific peptide with the sequence CSHSCTVP VTQECLF was synthesized at the Unit of Synthesis of Peptides (U3) of ICTS-NANBIOSIS, as part of the Custom Antibody Service (CAbS) at the Instituto de Química Avanzada de Cataluña - Consejo Superior de Investigaciones Científicas (IQAC-CSIC). The peptide was purified and conjugated to TRAN-KLH(CUCCA) B4, and the purified conjugated peptide was injected into three New Zealand rabbits following a standard immunization procedure of CAbS. Indirect ELISA assays were performed to assess the titer of rabbit antisera.

RNA extraction, semiquantitative RT-PCR, and real-time qRT-PCR

RNA extraction, reverse transcription, semiquantitative RT-PCR, and real-time qRT-PCR were performed as described previously.[70] For *PKM* splicing analysis, *GAPDH* transcript levels were used as CNTs, whereas for qRT-PCR, *GAPDH*, *GPI*, and *HPRT1* were used as endogenous references. Primer sequences are as in Sabater-Arcis et al.[70] *TNPO3*-specific primers are described by Blázquez-Bernal et al.[6] All experiments included three experimental samples. In qRT-PCR, three technical replicates from each sample were performed, and expression levels were normalized to the mean of reference genes using the comparative cycle threshold (Ct) method ($2^{-\Delta\Delta Ct}$ method).[71]

Western blotting

Protein extraction, quantification, and immunodetection of ATG7, LC3, and P62 were performed as previously described by Bargiela et al.[57] and Sabater-Arcis et al.[70] Specifically, TNPO3 and TNPO3mut were detected by denaturing 30 μg of total protein for 5 min at 100 °C, electrophoresed on 12% SDS-PAGE gels, and transferred onto 0.45 μm nitrocellulose membranes (GE Healthcare Life Sciences, Pittsburgh, PA, USA). Membranes were blocked with 5% non-fat dried milk in PBS-T (0.05% Tween 20 [pH 7.4] in PBS) for 1 h at room temperature (RT), then incubated overnight (ON) at 4 °C in a 5% blocking solution with primary antibodies dilutions. Specific primary antibodies used for blotting were mouse anti-TNPO3 (1:1,000; Abcam, Cambridge, UK), rabbit anti-TNPO3mut (1:1,000; this work), and mouse anti-β-Actin antibody (1:3,500; Sigma-Aldrich) as the loading CNT. Goat horseradish peroxidase (HRP)-conjugated anti-mouse IgG (1:3,500; Sigma-Aldrich) and goat HRP-conjugated anti-rabbit IgG (1:5,000; Sigma-Aldrich) were used as secondary antibodies and incubated for 1 h at RT.

Immunoreactive bands were detected using enhanced chemiluminescence western blotting substrate (Pierce, Thermo Fisher Scientific, Waltham, MA, USA), and images were taken in an ImageQuant LAS 4000 (GE Healthcare, Pittsburgh, PA, USA). Quantification was performed using ImageJ software (NIH).[68]

Immunofluorescence methods

For all immunodetections, 2.5×10^4 myoblasts/well were seeded in 24-well plates, and cells were fixed with 4% paraformaldehyde for 15 min at days 0 and 7 of differentiation. TNPO3 immunodetection was performed by adapting the protocol described by Costa et al.[11] In brief, fixed cells were permeabilized 5 min with PBS-T (0.2% Triton X-100 in PBS). After three washes with PBS, cells were blocked (PBS, 1% BSA, 1% normal goat serum [NGS]) for 1 h and incubated with rabbit anti-TNPO3 (1:200; ab71388; Abcam) ON at 4 °C. After three washes, cells were incubated for 1 h at 37 °C with goat anti-rabbit IgG (H + L) Alexa Fluor Plus 594 (1:200; A32740; ThermoFisher Scientific) in blocking buffer. Finally, cells were washed thrice and were mounted.

For Desmin and MHC immunodetection, fixed cells were washed three times with PBS-T2 (0.1% Triton X-100 in PBS); cells were blocked (PBS-T2, 1% BSA, 1% NGS) for 1 h and then incubated ON at 4 °C in blocking buffer with primary antibodies at the appropriate dilution. Specific primary antibodies were rabbit anti-Desmin (1:200; ab15200; Abcam, Cambridge, UK) and mouse anti-MHC (1:50; MF-20; Developmental Studies Hybridoma Bank, University of Iowa, IA, USA). After three washes with PBS-T, cells were incubated for 2 h at RT with secondary antibodies diluted in blocking buffer: goat anti-rabbit IgG (H + L) Alexa Fluor Plus 488 (1:200; A32731; ThermoFisher Scientific), and goat anti-Mouse IgG (H + L) Alexa Fluor Plus 488 (1:200; A32723; ThermoFisher Scientific). After triple wash, cells were mounted.

To detect the nuclei, we mounted all samples with VECTASHIELD mounting medium containing 4′,6-diamidino-2-phenylindole (DAPI; Vector Laboratories, CA, USA). Images were taken at 200× magnification for Desmin and MHC immunodetection and at 400× magnification for TNPO3, LC3, and LysoTracker staining, using an LSM800 confocal microscope (Zeiss, Jena, Germany).

Fusion index and myotube diameter were quantified by adapting the method described by Bargiela et al.[57] and Sabater-Arcis et al.[70] In brief, myotube diameter was measured at five points along the entire tube, and the mean diameter per micrograph was calculated. A total of 15–20 images were analyzed per condition. The percentage of nuclei within MHC^+ myotubes was obtained relative to the total number of nuclei in each condition. LC3 immunostaining, LC3 puncta quantification, and LysoTracker staining were performed as described by Sabater-Arcis et al.[38] All quantifications used ImageJ software (NIH).[68]

RNA-seq, data analysis, and functional annotation

RNA-seq was performed on the NovaSeq 6000 Illumina platform (Novogene, China). FastQ files were inspected using FastQC (FastQC: A Quality Control Tool for High Throughput Sequence Data).[72] For the RNA-seq analysis, FastQ sequences were mapped against the Genome Reference Consortium Human Build 38 (GRCh38.p13) and the Genome Reference Consortium Mice Build 39 (GRCm39) in the case of the murine *Cdk-4* gene quantification. The software used for mapping was STAR (version 2.7.3).[73] The RNA-seq by Expectation Maximization (RSEM)[74] (version 1.3.2) was used to produce the count table for each sample. RSEM algorithm was chosen because it is optimized for multi-mapped reads. The RNA-seq analysis was performed using the R software (version 3.6.3) with edgeR.[75] Only genes with a count per million greater than 1 in at least two samples were considered. The raw counts were normalized using the trimmed mean of M values algorithm.[76] Statistical testing was done using the empirical Bayes quasi-likelihood F test. The normalized counts were then transformed into a $\log_2$ fold-change (FC) table with their associated statistics, p value, and false discovery rate (FDR). Genes with a $|\log_2 FC| > 1$ and an FDR < 0.05 were considered as significantly differentially expressed. A $|\log_2 FC| > 1$ means at least two times more or two times less transcript in the test group in comparison with the CNT group. RNA-seq data are publicly available in the Gene Expression Omnibus (GEO) repository with accession number GEO: GSE198551.

ORA was performed for functional annotation using ClusterProfiler R packages.[77,78] The gene set used for this analysis was the recovered gene list, and all terms with a p value < 0.05 were considered statistically significant.

Identification and quantification of miRNAs were performed using the sRNA analysis suite sRNAtoolbox.[79] We used sRNAbench with the human miRNA database miRBase 22.1 and the human assembly GRCh38_p13. Differential expression was calculated using edger,[75] and miRNAs were considered significatively altered if FDR < 0.05.

STR profiling

The experiment was carried out by the company STABVIDA. In brief, genomic DNA from primary and immortalized LGMDD2 myoblasts was sequenced by multiplex PCR using Powerplex 16 loci kit (Promega, Madison, WI, USA). Results were analyzed by GeneMarker HID v1.75.

Cell proliferation assay

A total of 5×10^3 primary and immortalized myoblasts per well were seeded in 96-well plates and were incubated at 37 °C in a humidified chamber with 5% CO_2 for 24, 48, 72, and 96 h in growth medium. To measure cell proliferation, we added 20 μL of solution of tetrazolium compound ([3-(4,5-dimethylthiazol-2-yl)-5-(3-carboxymethoxyphenyl)-2-(4-sulfophenyl)-2H-tetrazolium, inner salt; MTS), and an electron coupling reagent (phenazine methosulfate [PMS]) was added to each well, which contained 100 μL of medium, and was incubated for 4 h. The conversion of MTS into soluble formazan was measured by absorbance at 490 nm (CellTiter 96 aqueous non-radioactive cell

proliferation assay; Promega). Absorbance was measured using an Infinite 200 PRO plate reader (Tecan Life Sciences, Männedorf, Switzerland).

mCherry-eGFP reporters fluorescence assays

Tandem mCherry-EGFP reporter assay was performed by adapting the protocol described by Sabater-Arcis et al.[70] A total of 2.5×10^4 immortalized myoblasts per well were seeded in 24-well plates. At 48 h of differentiation, myoblasts were transiently transfected with 1 μg of pDest-mCherry-eGFP-LC3B or pDest-mCherry-eGFP-P62 (kindly provided by Prof. Fuentes, University of Extremadura, Spain) using X-tremeGENE HP DNA transfection reagent (Roche Life Science) following the manufacturer's recommendations in Opti-MEM (Gibco) for 24 h. Then, differentiation medium was replaced, and after 48 h differentiated myoblasts were visualized *in vivo* using LSM800 confocal microscope (Zeiss, Jena, Germany) at 400× magnification. In the case of CQ treatment as control, myoblasts were incubated with CQ 10 μM 16 h before visualizing the cells.

Statistical analyses

All statistical analyses were performed using GraphPad Prism 9 software. The results of each experiment were represented by a scatterplot with bars. Data points correspond to the individual values in each condition. Sample sizes (n) are included in the figure legends. For volcano plots, each point represents one gene or miRNA. In all molecular studies, for comparison of normalized data means, we assumed that all parameters followed a normal distribution. For comparisons of two conditions, it was applied with two-tailed Student's t test ($\alpha = 0.05$) and Welch's correction when necessary. Statistical significance was set to $p < 0.05$. For multiple comparisons, normalized data were compared using Fisher's least significant difference (LSD) test of one-way ANOVA test ($\alpha = 0.05$).

DATA AVAILABILITY STATEMENT

All data supporting the findings of this study are available. Raw data are available on request.

SUPPLEMENTAL INFORMATION

Supplemental information can be found online at https://doi.org/10.1016/j.omtn.2023.01.004.

ACKNOWLEDGMENTS

This work was supported by the LGMDD2 patient association "Asociación Conquistando Escalones." The authors wish to thank Conquistando Escalones for their enormous effort in securing funding, their trust in our work, and extraordinary cooperation. J.P.-G. was supported by a grant from Fundación Isabel Gemio (Madrid, Spain). Additional funding was from a research grant by Fundación Feder (AI-2021-003), MCIN/AEI/10.13039/501100011033 (PID2021-125978OB-C22), and from "ERDF A way of making Europe" by the "European Union" (to R.A.). A.B. is grateful for the support of the Instituto de Salud Carlos III, Ministry of Science and Innovation, as a Sara Borrell postdoctoral grantee (CD21/00031). J.E.-E. was supported by predoctoral fellowship GRISOLIAP/2018/098 from the Conselleria d'Educació, Investigació, Cultura i Esport (Generalitat Valenciana). The equipment used in this research was partly funded by Generalitat Valenciana and co-financed with ERDF funds (OP ERDF of Comunitat Valenciana 2014–2020). R.P.V.-M. used for this work grants funded by the ISCIII (PI17/00011 and PI20/00114); these grants are co-financed by the European Development Regional Fund "A way to achieve Europe" (ERDF). Funds from the Fundación Ramón Areces were also used (CIVP19S8119).

AUTHOR CONTRIBUTIONS

Conception and design, R.A., J.J.V., A.B., and R.P.V.-M.; financial support, R.A. and J.J.V.; investigation, J.P.-G., A.B.-B., and M.S.-G.; collection and/or assembly of data, J.P.-G., A.B.-B., M.S.-G., and J.E.-E.; data analysis and interpretation, A.B.-B., J.P.-G., and A.B.; manuscript writing, A.B. and A.B.-B.; review and final approval of the manuscript, J.J.V. and R.A.

DECLARATION OF INTERESTS

The authors declare no competing interests.

REFERENCES

1. Gamez, J., Navarro, C., Andreu, A.L., Fernandez, J.M., Palenzuela, L., Tejeira, S., Fernandez-Hojas, R., Schwartz, S., Karadimas, C., DiMauro, S., et al. (2001). Autosomal dominant limb-girdle muscular dystrophy: a large kindred with evidence for anticipation. Neurology *56*, 450–454.

2. Melià, M.J., Kubota, A., Ortolano, S., Vílchez, J.J., Gámez, J., Tanji, K., Bonilla, E., Palenzuela, L., Fernández-Cadenas, I., Pristoupilová, A., et al. (2013). Limb-girdle muscular dystrophy 1F is caused by a microdeletion in the transportin 3 gene. Brain *136*, 1508–1517.

3. Torella, A., Fanin, M., Mutarelli, M., Peterle, E., Del Vecchio Blanco, F., Rispoli, R., Savarese, M., Garofalo, A., Piluso, G., Morandi, L., et al. (2013). Next-generation sequencing identifies transportin 3 as the causative gene for LGMD1F. PLoS One *8*, e63536–e63537.

4. Vihola, A., Palmio, J., Danielsson, O., Penttilä, S., Louiselle, D., Pittman, S., Weihl, C., and Udd, B. (2019). Novel mutation in TNPO3 causes congenital limb-girdle myopathy with slow progression. Neurol. Genet. *5*, e337–e339.

5. Pál, E., Zima, J., Hadzsiev, K., Ito, Y.A., Hartley, T., Care4Rare Canada Consortium, Boycott, K.M., and Melegh, B. (2019). A novel pathogenic variant in TNPO3 in a Hungarian family with limb-girdle muscular dystrophy 1F. Eur. J. Med. Genet. *62*, 103662.

6. Blázquez-Bernal, Á., Fernandez-Costa, J.M., Bargiela, A., and Artero, R. (2021). Inhibition of autophagy rescues muscle atrophy in a LGMDD2 Drosophila model. Faseb. J. *35*.

7. Gibertini, S., Ruggieri, A., Saredi, S., Salerno, F., Blasevich, F., Napoli, L., Moggio, M., Nigro, V., Morandi, L., Maggi, L., and Mora, M. (2018). Long term follow-up and further molecular and histopathological studies in the LGMD1F sporadic TNPO3-mutated patient. Acta Neuropathol. Commun. *6*, 141.

8. Maertens, G.N., Cook, N.J., Wang, W., Hare, S., Gupta, S.S., Öztop, I., Lee, K., Pye, V.E., Cosnefroy, O., Snijders, A.P., et al. (2014). Structural basis for nuclear import of splicing factors by human Transportin 3. Proc. Natl. Acad. Sci. USA *111*, 2728–2733.

9. Lai, M.-C., Lin, R.-I., Huang, S.-Y., Tsai, C.-W., and Tarn, W.-Y. (2000). A human importin-β family protein, transportin-SR2, interacts with the phosphorylated RS domain of SR proteins. J. Biol. Chem. *275*, 7950–7957.

10. Rodríguez-Mora, S., De Wit, F., García-Perez, J., Bermejo, M., López-Huertas, M.R., Mateos, E., Martí, P., Rocha, S., Vigón, L., Christ, F., et al. (2019). The mutation of Transportin 3 gene that causes limb girdle muscular dystrophy 1F induces protection against HIV-1 infection. PLoS Pathog. *15*, e1007958.

11. Costa, R., Rodia, M.T., Zini, N., Pegoraro, V., Marozzo, R., Capanni, C., Angelini, C., Lattanzi, G., Santi, S., and Cenacchi, G. (2021). Morphological study of TNPO3 and SRSF1 interaction during myogenesis by combining confocal, structured illumination and electron microscopy analysis. Mol. Cell. Biochem. *476*, 1797–1811.

12. Costa, R., Rodia, M.T., Vianello, S., Santi, S., Lattanzi, G., Angelini, C., Pegoraro, E., and Cenacchi, G. (2020). Transportin 3 (TNPO3) and related proteins in limb girdle muscular dystrophy D2 muscle biopsies: a morphological study and pathogenetic hypothesis. Neuromuscul. Disord. *30*, 685–692.

13. Cenacchi, G., Peterle, E., Fanin, M., Papa, V., Salaroli, R., and Angelini, C. (2013). Ultrastructural changes in LGMD1F. Neuropathology *33*, 276–280.

14. Young, C.S., Pyle, A.D., and Spencer, M.J. (2019). CRISPR for neuromuscular disorders: gene editing and beyond. Physiology *34*, 341–353.

15. Mojica, F.J.M., Díez-Villaseñor, C., García-Martínez, J., and Soria, E. (2005). Intervening sequences of regularly spaced prokaryotic repeats derive from foreign genetic elements. J. Mol. Evol. *60*, 174–182.

16. Jinek, M., Chylinski, K., Fonfara, I., Hauer, M., Doudna, J.A., and Charpentier, E. (2012). A programmable dual-RNA–guided DNA Endonuclease in adaptive bacterial immunity. Science *337*, 816–821.

17. Mali, P., Yang, L., Esvelt, K.M., Aach, J., Guell, M., DiCarlo, J.E., Norville, J.E., and Church, G.M. (2013). RNA-guided human genome engineering via Cas9. Science *339*, 823–826.

18. Cong, L., Ran, F.A., Cox, D., Lin, S., Barretto, R., Habib, N., Hsu, P.D., Wu, X., Jiang, W., Marraffini, L.A., and Zhang, F. (2013). Multiplex genome engineering using CRISPR/Cas systems. Science *339*, 819–823.

19. Ran, F.A., Cong, L., Yan, W.X., Scott, D.A., Gootenberg, J.S., Kriz, A.J., Zetsche, B., Shalem, O., Wu, X., Makarova, K.S., et al. (2015). In vivo genome editing using Staphylococcus aureus Cas9. Nature *520*, 186–191.

20. Turan, S., Farruggio, A.P., Srifa, W., Day, J.W., and Calos, M.P. (2016). Precise correction of disease mutations in induced pluripotent stem cells derived from patients with limb girdle muscular dystrophy. Mol. Ther. *24*, 685–696.

21. Mamchaoui, K., Trollet, C., Bigot, A., Negroni, E., Chaouch, S., Wolff, A., Kandalla, P.K., Marie, S., Di Santo, J., St Guily, J.L., et al. (2011). Immortalized pathological human myoblasts: towards a universal tool for the study of neuromuscular disorders. Skeletal Muscle *1*, 34.

22. Oliveros, J.C., Franch, M., Tabas-Madrid, D., San-León, D., Montoliu, L., Cubas, P., and Pazos, F. (2016). Breaking-Cas—interactive design of guide RNAs for CRISPR-Cas experiments for ENSEMBL genomes. Nucleic Acids Res. *44*, W267–W271.

23. Kim, S., Kim, D., Cho, S.W., Kim, J., and Kim, J.-S. (2014). Highly efficient RNA-guided genome editing in human cells via delivery of purified Cas9 ribonucleoproteins. Genome Res. *24*, 1012–1019.

24. Gong, C., Bongiorno, P., Martins, A., Stephanou, N.C., Zhu, H., Shuman, S., and Glickman, M.S. (2005). Mechanism of nonhomologous end-joining in mycobacteria: a low-fidelity repair system driven by Ku, ligase D and ligase C. Nat. Struct. Mol. Biol. *12*, 304–312.

25. Chen, F., Pruett-Miller, S.M., Huang, Y., Gjoka, M., Duda, K., Taunton, J., Collingwood, T.N., Frodin, M., and Davis, G.D. (2011). High-frequency genome editing using ssDNA oligonucleotides with zinc-finger nucleases. Nat. Methods *8*, 753–755.

26. Radecke, S., Radecke, F., Cathomen, T., and Schwarz, K. (2010). Zinc-finger nuclease-induced gene repair with oligodeoxynucleotides: wanted and unwanted target locus modifications. Mol. Ther. *18*, 743–753.

27. Brinkman, E.K., Chen, T., Amendola, M., and van Steensel, B. (2014). Easy quantitative assessment of genome editing by sequence trace decomposition. Nucleic Acids Res. *42*, e168.

28. Sentmanat, M.F., Peters, S.T., Florian, C.P., Connelly, J.P., and Pruett-Miller, S.M. (2018). A survey of validation strategies for CRISPR-cas9 editing. Sci. Rep. *8*, 888.

29. Angelini, C., Marozzo, R., Pinzan, E., Pegoraro, V., Molnar, M.J., Torella, A., and Nigro, V. (2019). A new family with transportinopathy: increased clinical heterogeneity. Ther. Adv. Neurol. Disord. *12*. 1756286419850433.

30. Cisternas, P., Henriquez, J.P., Brandan, E., and Inestrosa, N.C. (2014). Wnt signaling in skeletal muscle dynamics: myogenesis, neuromuscular synapse and fibrosis. Mol. Neurobiol. *49*, 574–589.

31. Yedigaryan, L., and Sampaolesi, M. (2021). Therapeutic implications of miRNAs for muscle-wasting conditions. Cells *10*, 3035.

32. Gandhi, G., Abdullah, S., Foead, A.I., and Yeo, W.W.Y. (2021). The potential role of miRNA therapies in spinal muscle atrophy. J. Neurol. Sci. *427*, 117485.

33. Koutsoulidou, A., Kyriakides, T.C., Papadimas, G.K., Christou, Y., Kararizou, E., Papanicolaou, E.Z., and Phylactou, L.A. (2015). Elevated muscle-specific miRNAs in serum of myotonic dystrophy patients relate to muscle disease progress. PLoS One *10*, e0125341.

34. van der Plas, E., Gutmann, L., Thedens, D., Shields, R.K., Langbehn, K., Guo, Z., Sonka, M., and Nopoulos, P. (2021). Quantitative muscle MRI as a sensitive marker of early muscle pathology in myotonic dystrophy type 1. Muscle Nerve *63*, 553–562.

35. Gao, Z., and Cooper, T.A. (2013). Reexpression of pyruvate kinase M2 in type 1 myofibers correlates with altered glucose metabolism in myotonic dystrophy. Proc. Natl. Acad. Sci. USA *110*, 13570–13575.

36. Guglieri, M., Straub, V., Bushby, K., and Lochmüller, H. (2008). Limb–girdle muscular dystrophies. Curr. Opin. Neurol. *21*, 576–584.

37. Spreafico, M., Cafora, M., Bragato, C., Capitanio, D., Marasca, F., Bodega, B., De Palma, C., Mora, M., Gelfi, C., Marozzi, A., and Pistocchi, A. (2021). Targeting HDAC8 to ameliorate skeletal muscle differentiation in Duchenne muscular dystrophy. Pharmacol. Res. *170*, 105750.

38. Sabater-Arcis, M., Bargiela, A., Moreno, N., Poyatos-Garcia, J., Vilchez, J.J., and Artero, R. (2021). Musashi-2 contributes to myotonic dystrophy muscle dysfunction by promoting excessive autophagy through miR-7 biogenesis repression. Mol. Ther. Nucleic Acids *25*, 652–667.

39. Chal, J., and Pourquié, O. (2017). Making muscle: skeletal myogenesis in vivo and in vitro. Development *144*, 2104–2122.

40. Tanida, I., Ueno, T., and Kominami, E. (2008). LC3 and autophagy. Methods Mol. Biol. *445*, 77–88.

41. Collier, J.J., Suomi, F., Oláhová, M., McWilliams, T.G., and Taylor, R.W. (2021). Emerging roles of ATG7 in human health and disease. EMBO Mol. Med. *13*, e14824.

42. Bjørkøy, G., Lamark, T., Pankiv, S., Øvervatn, A., Brech, A., and Johansen, T. (2009). Monitoring autophagic degradation of p62/SQSTM1. Methods Enzymol. *452*, 181–197.

43. Rusten, T.E., and Stenmark, H. (2010). p62, an autophagy hero or culprit? Nat. Cell Biol. *12*, 207–209.

44. Klionsky, D.J., Abdel-Aziz, A.K., Abdelfatah, S., Abdellatif, M., Abdoli, A., Abel, S., Abeliovich, H., Abildgaard, M.H., Abudu, Y.P., Acevedo-Arozena, A., et al. (2014). Guidelines for the use and interpretation of assays for monitoring autophagy. Autophagy *10*, 1691–2382.

45. Larue, R., Gupta, K., Wuensch, C., Shkriabai, N., Kessl, J.J., Danhart, E., Feng, L., Taltynov, O., Christ, F., Van Duyne, G.D., et al. (2012). Interaction of the HIV-1 intasome with transportin 3 protein (TNPO3 or TRN-SR2). J. Biol. Chem. *287*, 34044–34058.

46. Diez-Fuertes, F., López-Huertas, M.R., García-Pérez, J., Calonge, E., Bermejo, M., Mateos, E., Martí, P., Muelas, N., Vílchez, J.J., Coiras, M., et al. (2022). Transcriptomic evidence of the immune response activation in individuals with limb girdle muscular dystrophy dominant 2 (LGMDD2) contributes to resistance to HIV-1 infection. Front. Cell Dev. Biol. *10*, 839813.

47. Mukherjee, S., and Zhang, Y. (2011). Protein-protein complex structure predictions by multimeric threading and template recombination. Structure *19*, 955–966.

48. Jeong, S. (2017). SR proteins: binders, regulators, and connectors of RNA. Mol. Cell *40*, 1–9.

49. Nakka, K., Ghigna, C., Gabellini, D., and Dilworth, F.J. (2018). Diversification of the muscle proteome through alternative splicing. Skeletal Muscle *8*, 8.

50. López-Martínez, A., Soblechero-Martín, P., De-la-Puente-Ovejero, L., Nogales-Gadea, G., and Arechavala-Gomeza, V. (2020). An overview of alternative splicing defects implicated in myotonic dystrophy type I. Genes *11*, 1109.

51. Wei, N., Cheng, Y., Wang, Z., Liu, Y., Luo, C., Liu, L., Chen, L., Xie, Z., Lu, Y., and Feng, Y. (2015). SRSF10 plays a role in myoblast differentiation and glucose production via regulation of alternative splicing. Cell Rep. *13*, 1647–1657.

52. Lv, Y., Zhang, W., Zhao, J., Sun, B., Qi, Y., Ji, H., Chen, C., Zhang, J., Sheng, J., Wang, T., et al. (2021). SRSF1 inhibits autophagy through regulating Bcl-x splicing and interacting with PIK3C3 in lung cancer. Signal Transduct. Targeted Ther. *6*, 108.

53. Singh, A., Phogat, J., Yadav, A., and Dabur, R. (2021). The dependency of autophagy and ubiquitin proteasome system during skeletal muscle atrophy. Biophys. Rev. *13*, 203–219.

54. Franekova, V., Storjord, H.I., Leivseth, G., and Nilssen, Ø. (2021). Protein homeostasis in LGMDR9 (LGMD2I) – the role of ubiquitin–proteasome and autophagy–lysosomal system. Neuropathol. Appl. Neurobiol. *47*, 519–531.

55. Fanin, M., Nascimbeni, A.C., and Angelini, C. (2013). Muscle atrophy in L imb G irdle M uscular D ystrophy 2 A : a morphometric and molecular study. Neuropathol. Appl. Neurobiol. *39*, 762–771.

56. Bargiela, A., Cerro-Herreros, E., Fernandez-Costa, J.M., Vilchez, J.J., Llamusi, B., and Artero, R. (2015). Increased autophagy and apoptosis contribute to muscle atrophy in a myotonic dystrophy type 1 Drosophila model. Dis. Model. Mech. *8*, 679–690.

57. Bargiela, A., Sabater-Arcis, M., Espinosa-Espinosa, J., Zulaica, M., Lopez de Munain, A., and Artero, R. (2019). Increased Muscleblind levels by chloroquine treatment improve myotonic dystrophy type 1 phenotypes in in vitro and in vivo models. Proc. Natl. Acad. Sci. USA *116*, 25203–25213.

58. Raben, N., Hill, V., Shea, L., Takikita, S., Baum, R., Mizushima, N., Ralston, E., and Plotz, P. (2008). Suppression of autophagy in skeletal muscle uncovers the accumulation of ubiquitinated proteins and their potential role in muscle damage in Pompe disease. Hum. Mol. Genet. *17*, 3897–3908.

59. Sharma, G., Sharma, A.R., Bhattacharya, M., Lee, S.-S., and Chakraborty, C. (2021). CRISPR-Cas9: a preclinical and clinical perspective for the treatment of human diseases. Mol. Ther. *29*, 571–586.

60. Amoasii, L., Hildyard, J.C.W., Li, H., Sanchez-Ortiz, E., Mireault, A., Caballero, D., Harron, R., Stathopoulou, T.-R., Massey, C., Shelton, J.M., et al. (2018). Gene editing restores dystrophin expression in a canine model of Duchenne muscular dystrophy. Science *362*, 86–91.

61. Kemaladewi, D.U., Maino, E., Hyatt, E., Hou, H., Ding, M., Place, K.M., Zhu, X., Bassi, P., Baghestani, Z., Deshwar, A.G., et al. (2017). Correction of a splicing defect in a mouse model of congenital muscular dystrophy type 1A using a homology-directed-repair-independent mechanism. Nat. Med. *23*, 984–989.

62. Pinto, B.S., Saxena, T., Oliveira, R., Méndez-Gómez, H.R., Cleary, J.D., Denes, L.T., McConnell, O., Arboleda, J., Xia, G., Swanson, M.S., and Wang, E.T. (2017). Impeding transcription of expanded microsatellite repeats by deactivated Cas9. Mol. Cell *68*, 479–490.e5.

63. Wang, X., Liu, Q., and Zhang, B. (2014). Leveraging the complementary nature of RNA-Seq and shotgun proteomics data. Proteomics *14*, 2676–2687.

64. Dastidar, S., Ardui, S., Singh, K., Majumdar, D., Nair, N., Fu, Y., Reyon, D., Samara, E., Gerli, M.F.M., Klein, A.F., et al. (2018). Efficient CRISPR/Cas9-mediated editing of trinucleotide repeat expansion in myotonic dystrophy patient-derived iPS and myogenic cells. Nucleic Acids Res. *46*, 8275–8298.

65. Cacchiarelli, D., Legnini, I., Martone, J., Cazzella, V., D'Amico, A., Bertini, E., and Bozzoni, I. (2011). miRNAs as serum biomarkers for Duchenne muscular dystrophy. EMBO Mol. Med. *3*, 258–265.

66. Perbellini, R., Greco, S., Sarra-Ferraris, G., Cardani, R., Capogrossi, M.C., Meola, G., and Martelli, F. (2011). Dysregulation and cellular mislocalization of specific miRNAs in myotonic dystrophy type 1. Neuromuscul. Disord. *21*, 81–88.

67. Fuster-García, C., García-García, G., González-Romero, E., Jaijo, T., Sequedo, M.D., Ayuso, C., Vázquez-Manrique, R.P., Millán, J.M., and Aller, E. (2017). USH2A gene editing using the CRISPR system. Mol. Ther. Nucleic Acids *8*, 529–541.

68. Schneider, C.A., Rasband, W.S., and Eliceiri, K.W. (2012). NIH Image to ImageJ: 25 years of image analysis. Nat. Methods *9*, 671–675.

69. Soblechero-Martín, P., Albiasu-Arteta, E., Anton-Martinez, A., de la Puente-Ovejero, L., Garcia-Jimenez, I., González-Iglesias, G., Larrañaga-Aiestaran, I., López-Martínez, A., Poyatos-García, J., Ruiz-Del-Yerro, E., et al. (2021). Duchenne muscular dystrophy cell culture models created by CRISPR/Cas9 gene editing and their application in drug screening. Sci. Rep. *11*, 18188.

70. Sabater-Arcis, M., Bargiela, A., Furling, D., and Artero, R. (2020). miR-7 restores phenotypes in myotonic dystrophy muscle cells by repressing hyperactivated autophagy. Mol. Ther. Nucleic Acids *19*, 278–292.

71. Livak, K.J., and Schmittgen, T.D. (2001). Analysis of relative gene expression data using real-time quantitative PCR and the 2-ΔΔCT method. Methods *25*, 402–408.

72. Babraham bioinformatics - FastQC A quality control tool for high Throughput sequence data. https://www.bioinformatics.babraham.ac.uk/projects/fastqc/.

73. Dobin, A., Davis, C.A., Schlesinger, F., Drenkow, J., Zaleski, C., Jha, S., Batut, P., Chaisson, M., and Gingeras, T.R. (2013). STAR: ultrafast universal RNA-seq aligner. Bioinformatics *29*, 15–21.

74. Li, B., and Dewey, C.N. (2011). RSEM: accurate transcript quantification from RNA-Seq data with or without a reference genome. BMC Bioinf. *12*, 323.

75. Robinson, M.D., McCarthy, D.J., and Smyth, G.K. (2010). edgeR: a Bioconductor package for differential expression analysis of digital gene expression data. Bioinformatics *26*, 139–140.

76. Robinson, M.D., and Oshlack, A. (2010). A scaling normalization method for differential expression analysis of RNA-seq data. Genome Biol. *11*, R25.

77. Wu, T., Hu, E., Xu, S., Chen, M., Guo, P., Dai, Z., Feng, T., Zhou, L., Tang, W., Zhan, L., et al. (2021). clusterProfiler 4.0: a universal enrichment tool for interpreting omics data. Innovation *2*, 100141.

78. Yu, G., and He, Q.-Y. (2016). ReactomePA: an R/Bioconductor package for reactome pathway analysis and visualization. Mol. Biosyst. *12*, 477–479.

79. Aparicio-Puerta, E., Lebrón, R., Rueda, A., Gómez-Martín, C., Giannoukakos, S., Jaspez, D., Medina, J.M., Zubkovic, A., Jurak, I., Fromm, B., et al. (2019). sRNAbench and sRNAtoolbox 2019: intuitive fast small RNA profiling and differential expression. Nucleic Acids Res. *47*, W530–W535.